ChemPubSoc Europe

DOI: 10.1002/cctc.201501347

CHEMCATCHEM Full Papers

Direct Synthesis of TiO_2-Supported MoS_2 Nanoparticles by Reductive Coprecipitation

Lennart van Haandel,[a] John W. Geus,[b] and Thomas Weber*[a]

Molybdenum disulfide nanoparticles supported on titania were synthesized from aqueous solutions containing Ti and Mo precursor salts by an in situ redox reaction. The synthesis involves a redox process between Ti^{3+} and MoS_4^{2-}, which proceeds readily under mild conditions in aqueous solution. Catalysts were made in a single step, yielding amorphous catalysts with high Mo content, or in two steps to obtain MoS_2 supported on well-defined TiO_2 with lower Mo content. Catalysts obtained by single-step reductive coprecipitation were highly active in the hydrodesulfurization of dibenzothiophene, exceeding the activity of an alumina-supported Co–Mo reference. In contrast to alumina-supported catalysts, the addition of Co as promoter did not enhance the catalytic activity of MoS_2/TiO_2 to the same extent (+30%) as for alumina-supported Co–Mo catalysts. Instead, a change in selectivity towards hydrogenolysis products at the expense of hydrogenation products was observed. It is suggested that Ti may act as a promoter for MoS_2 in hydrogenation reactions.

Introduction

The synthesis of industrial heterogeneous catalysts, composed of highly dispersed active nanoparticles on a porous support, usually involves multiple steps.[1] Typically, the support is prepared and shaped first and subsequently loaded with the desired metal salt precursors. Several steps of drying, calcination, and activation are then required to obtain the catalytically active phase, each exhibiting some inherent drawbacks. For example, during drying the precursor may migrate and agglomerate at the pore mouth. Calcination can lead to incorporation of the precursor into the support and activation may lead to initial sintering of metal nanoparticles, resulting in a loss of catalytic activity and/or selectivity.[1,2] The development of synthetic routes that involve fewer steps is thus not only economically attractive, but it may also lead to a higher degree of control over materials properties.

Several one-step methodologies have been reported for the synthesis of heterogeneous catalysts containing noble[3] or non-noble[3b,4] metal nanoparticles. However, despite their simplified preparation, calcination and/or reduction may still be required to obtain the catalyst in its active state. Reduction by H_2 or other reducing agents such as $NaBH_4$ can be circumvented if the support facilitates reduction directly. Redox-active supports (or their precursors) such as CeO_2 and TiO_2 are capable of reducing noble-metal salts in solution to obtain supported metallic nanoparticles directly.[5] Such an approach has not yet been demonstrated for non-noble metals, although the deposition of small amounts of MS_2 (M = Mo, W) on TiO_2 by photoreduction has suggested that a similar approach may work for transition-metal disulfides (TMS).[6]

TMS are an important class of materials that have attracted interest in a variety of fields such as catalysis and energy storage.[7] In particular, they are broadly applied in refineries to catalyze the removal of heteroatoms (S, N, O, Ni, V, etc.) from oil. Hydrotreating (HDT) catalysts are typically composed of Co- or Ni- promoted MoS_2 nanoparticles supported on γ-Al_2O_3.[8] Several researchers have reported that TiO_2 as a support improves intrinsic hydrodesulfurization (HDS) performance by a factor of four to five.[9] Nevertheless, practical applications of TiO_2 as a support in HDS catalysts are limited by its maximum Mo loading, which is constrained by the lower surface area compared with Al_2O_3.[9a,10]

Several strategies were proposed to overcome the low Mo capacity of TiO_2. These strategies include the synthesis of high-surface-area TiO_2,[10] mixed supports of TiO_2 with other metal oxides (ZrO_2, Al_2O_3, and SiO_2),[11] and the synthesis of TiO_2-coated Al_2O_3.[12] Despite the higher Mo loadings accommodated by these supports, in all cases Co and Mo were added by post-impregnation. Recently, Nguyen et al. reported a single-step synthesis of TiO_2-supported Co–Mo oxide HDT catalyst precursors by a sol–gel method.[13] By this approach, the Mo loading could be varied up to 30 wt.%. A drawback of this method was that part of the Mo was incorporated in the support and remained unsulfided. Consequently, the samples prepared by the sol–gel method were less active than impregnated samples with the same Mo loading.

[a] L. van Haandel, Prof. Dr. T. Weber
Shell Technology Centre Amsterdam
Shell Projects & Technology/Criterion Catalysts
Grasweg 31
1031 HW Amsterdam (The Netherlands)
E-mail: thomas.t.weber@shell.com

[b] Prof. J. W. Geus
Debye Institute for Nanomaterials, Faculty of Science
Utrecht University
Universiteitsweg 99
3584 CG Utrecht (The Netherlands)

Supporting Information for this article can be found under http://dx.doi.org/10.1002/cctc.201501347.

In this work we report the direct synthesis of nonpromoted and Co-promoted MoS_2 nanoparticles supported on TiO_2 (MoS_2/TiO_2 and $Co–MoS_2/TiO_2$, respectively) by reductive coprecipitation (RCP). The synthesis involves a redox reaction between Ti^{3+} and MoS_4^{2-} in aqueous solution and proceeds readily under mild conditions. To our knowledge, this is the first example of simultaneous formation of support and metal sulfide nanoparticles in a single step. Furthermore, unlike in the sol–gel method, we did not find evidence that coprecipitation leads to encapsulation of active MoS_2 particles by the support. The catalysts proved to be highly active in the HDS of dibenzothiophene (DBT) under mild conditions (40 bar, 245 °C), even in the absence of Co. The remarkable activity of the unpromoted catalyst, which is competitive with a commercial alumina-supported Co–Mo reference, can be attributed to an increased hydrogenation activity. This suggests that Ti (TiO_2) may act as a promoter for MoS_2 in hydrogenation reactions. The as-synthesized catalysts were characterized by transmission electron microscopy (TEM), energy-dispersive X-ray spectroscopy (EDX), X-ray diffraction (XRD), X-ray fluorescence (XRF), and X-ray photoelectron spectroscopy (XPS).

Results and Discussion

TiO_2-supported MoS_2 catalysts were synthesized from aqueous solutions of $(NH_4)_2MoS_4$ and $TiCl_3$ by reductive coprecipitation (RCP). The method involves hydrolysis and oxidation of $TiCl_3$ and simultaneous reduction and decomposition of $(NH_4)_2MoS_4$ to MoS_2 (Figure 1). The involved redox process is formally described by the following half-reactions:

$$2\,Ti^{3+} \rightarrow 2\,Ti^{4+} + 2\,e^- \quad (1)$$

$$Mo^{6+} + 2\,e^- \rightarrow Mo^{4+} \quad (2)$$

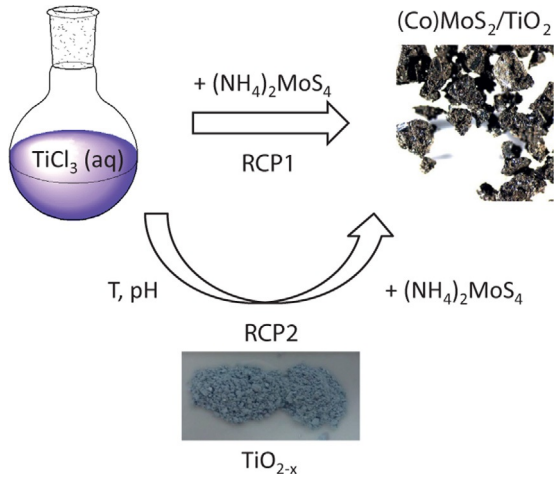

Figure 1. Schematic representation of the one-step (RCP1) and two-step (RCP2) reductive coprecipitation processes. In RCP1 the product forms directly in an aqueous solution of the precursor salts, whereas RCP2 involves preparation of TiO_{2-x} and subsequent loading with MoS_2.

Genesis of the supported catalysts is likely an interplay between redox, hydrolysis, and condensation reactions. $TiCl_3$ is hydrolyzed, and subsequently it condensates to form a gel-like structure, similarly to the early stage of TiO_2 synthesis from $TiCl_4$.[14] Simultaneously, Ti^{3+} is oxidized by MoS_4^{2-}, yielding MoS_2. We found that reduction of MoS_4^{2-} proceeds readily under mild acidic or neutral conditions. MoS_2 spontaneously precipitates upon addition of a neutral solution of Ti^{3+}, chelated by nitrilotriacetic acid, to a neutral solution of $(NH_4)_2MoS_4$ (see the Supporting Information and Figure S1). However, under alkaline conditions Ti^{3+} is rapidly oxidized by water or hydroxyl anions to Ti^{4+}. Consequently, MoS_2 does not form under these conditions.

Under acidic conditions, the reduction of MoS_4^{2-} by Ti^{3+} is in competition with its hydrolysis to MoS_3 [Eq. (3)], an amorphous Mo^{IV} solid, which cannot take part in the redox process anymore.[15]

$$Mo^{VI}S_4^{2-} + 2\,H_3O^+ \rightarrow Mo^{IV}S_3 + H_2S + 2\,H_2O \quad (3)$$

The formation of MoS_3 was suppressed by addition of a chelating agent (ethylenediaminetetraacetic acid, EDTA; or citric acid). The chelating agent stabilized Ti^{3+} ions in solution, allowing the reaction between Ti^{3+} and MoS_4^{2-} to proceed in acidic media. The optimum pH for synthesis was between 3 and 4, resulting in a nearly stoichiometric ratio of TiO_2 and MoS_2 (Table 1, entry 1).

Table 1. Properties of the as-synthesized catalysts.

Entry	Material	Mo [wt.%][a]	S/Mo ratio[b]	Mo/Ti ratio[b]	SSA [$m^2\,g^{-1}$]
1	MoS_2/TiO_2-RCP1	13.3	2.1	0.30	117
2	Co-MoS_2/TiO_2-RCP1	13.9	n.m.	n.m.	n.m.
3	MoS_2/TiO_2-RCP2-T	5.9	n.m.	n.m.	96
4	MoS_2/TiO_2-RCP2-H	3.2	2.5	0.04	129

[a] Sample 1 and 4 determined by XRF, sample 2 and 3 determined by ICP–OES. [b] molar ratio, n.m. = not measured.

Synthesis and characterization of TiO_{2-x} support

The supported catalysts were synthesized in a single step, either directly from a solution of the respective metal salts (RCP1) or from a dispersion of TiO_{2-x} support precursor in a solution of $(NH_4)_2MoS_4$ (RCP2). The TiO_{2-x} support precursor was prepared prior to the introduction of the $(NH_4)_2MoS_4$ salt. The advantage of this approach (RCP2) is that the morphology of the TiO_{2-x} support precursor can be modified by adjusting synthesis parameters (*T*, pH) without affecting the redox reaction between Ti^{3+} and MoS_4^{2-}, thus preventing unwanted side reactions.

Two methods were employed to synthesize TiO_{2-x} support precursors, thermolysis and hydrolysis. In the first method, thermolysis, TiO_{2-x} was synthesized overnight from an acidic $TiCl_3$ solution at 100 °C. In the second method, hydrolysis,

aqueous $TiCl_3$ was hydrolyzed by adding a base (1 M NaOH solution) and subsequently kept overnight at 60 °C to obtain TiO_{2-x}. Both methods yielded suspensions of fine blue TiO_{2-x} particles, which oxidized within one hour to TiO_2 when exposed to air. As such, it was important to keep TiO_{2-x} under inert atmosphere prior to reaction with thiomolybdate.

TEM images of TiO_2 particles obtained by thermolysis and hydrolysis are shown in Figure 2. Thermolysis yielded nanosized rods of approximately 200 nm in length that tended to form spherical aggregates. Electron diffraction (ED) confirmed that the particles were crystalline and were composed of the rutile polymorph, which was also confirmed by XRD spectroscopy (Figure S2). TiO_2 nanoparticles obtained by hydrolysis were approximately 25 nm in length and were polycrystalline. Both rutile and brookite were identified by their electron diffraction patterns, however, the presence of anatase could not be excluded.

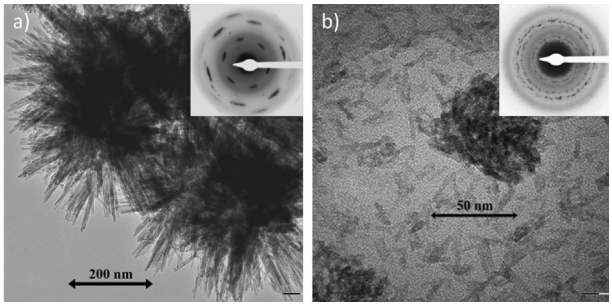

Figure 2. TEM images of TiO_2 prepared by a) thermolysis and b) hydrolysis. Insets: ED patterns.

Synthesis and characterization of MoS_2/TiO_2 catalysts

Four catalysts were prepared by the two RCP routes; their compositions are listed in Table 1. An unpromoted and a Co-promoted catalyst with high Mo loadings were prepared in a single step from aqueous solution by RCP1. The addition of Co during synthesis did not affect the redox process between Ti^{3+} and MoS_4^{2-} and yielded similar materials as far as the states of Ti and Mo are concerned. We will therefore only discuss the characterization of the unpromoted catalyst samples in the following paragraphs.

For RCP2 catalysts, TiO_{2-x} support precursors were synthesized either by thermolysis (RCP2-T) or hydrolysis (RCP2-H). Next, a solution of thiomolybdate was introduced, which was immediately reduced by the TiO_{2-x} phase to form MoS_2 nanoparticles on a TiO_2 surface. This procedure yielded catalysts with low Mo loadings, likely owing to the limited availability of Ti^{3+} on the TiO_{2-x} surface as indicated by the light blue color of the material. The specific surface areas (SSA) of catalysts prepared by RCP1 and RCP2 were comparable (100–130 $m^2 g^{-1}$, Table 1). The SSA data were obtained with MoS_2-loaded samples, which suggests that the SSA of TiO_2 synthesized by RCP is substantially higher than that of a typical TiO_2 support (P25, SSA = 50 $m^2 g^{-1}$).

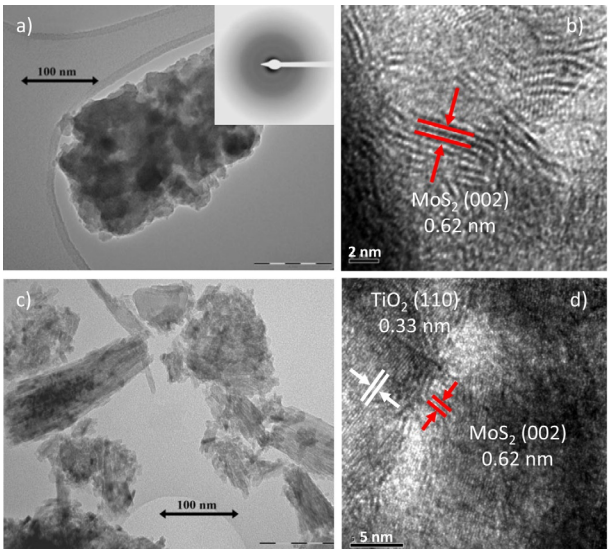

Figure 3. TEM images of a) MoS_2/TiO_2 prepared by RCP1 in water. Inset: ED pattern. b) HRTEM image of the same sample. the red lines indicate MoS_2 crystal lattice. c) MoS_2/TiO_2-RCP2-T. d) HRTEM image of the same sample. The (1 1 0) crystal lattice of rutile TiO_2 and stacked MoS_2 particles are indicated in white and red, respectively.

The TEM images in Figure 3 show catalysts synthesized by the RCP1 and RCP2 methods. The presence of crystalline TiO_2 or MoS_2 phases in MoS_2/TiO_2-RCP1 could not be confirmed by electron diffraction (ED, Figure 3a inset), indicating that the catalyst was mainly amorphous. A high-resolution TEM (HRTEM) image of the same particle revealed the presence of stacked MoS_2 layers with a characteristic d-spacing of 0.615 nm (Figure 3b). The TEM image of MoS_2/TiO_2-RCP2-T (Figure 3c) clearly shows deposits on the TiO_2 rods. Furthermore, the presence of MoS_2 in the same region was identified by HR-TEM (Figure 3d). This suggests that both synthesis methods successfully yielded MoS_2. No crystalline MoS_2 could be detected by XRD analysis, which may be attributed to the small particle size or disordered structure of the MoS_2 phase (Figure S2).

The homogeneity of MoS_2 on the support was evaluated by EDX spectroscopy and is shown in Figure 4. In both samples prepared by RCP1 and RCP2, the intensity of the Mo K and Ti K fluorescence lines varied simultaneously over the length of the linescan, indicating an even loading of Mo on TiO_2 (Figure 4, bottom right). The stoichiometry of S to Mo could not be determined directly by EDX analysis because the emission lines of the S K (2307 eV) and Mo L shell (2293 eV) overlapped. Instead, we compared the (S K + Mo L)/Mo K intensity ratio to that of bulk MoS_2 as displayed in Figure 4a. The obtained ratios for the samples were similar to that of bulk MoS_2, pointing to a successful reduction of thiomolybdate to MoS_2.

In Figure 5, the XP spectra of MoS_2/TiO_2-RCP1 and MoS_2/TiO_2-RCP2-T are compared with that of bulk MoS_2. The Mo 3d XP spectra reveal the presence of Mo in the 4+ and 6+ oxidation states. A lower binding energy (BE) was observed for the TiO_2-supported samples with respect to the bulk MoS_2 reference (Table 2). We attribute this shift in BE to electron donation from TiO_2 to MoS_2, which indicates a strong TMS–support inter-

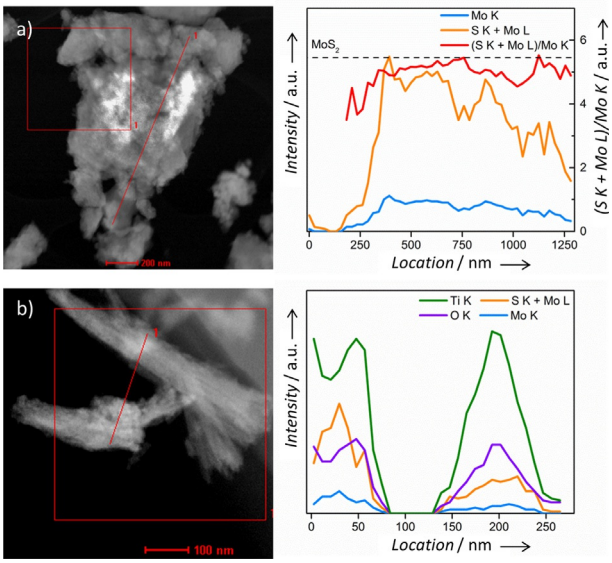

Figure 4. TEM–EDX linescan of a) MoS_2/TiO_2-RCP1 and b) MoS_2/TiO_2-RCP2-T. The linescan started at 1 and followed the red line as indicated in the TEM image (left) and the intensities of the emission lines are plotted on the right. The black dotted line indicates the intensity ratio of (S K + Mo L)/Mo K emission lines of a bulk MoS_2 reference sample.

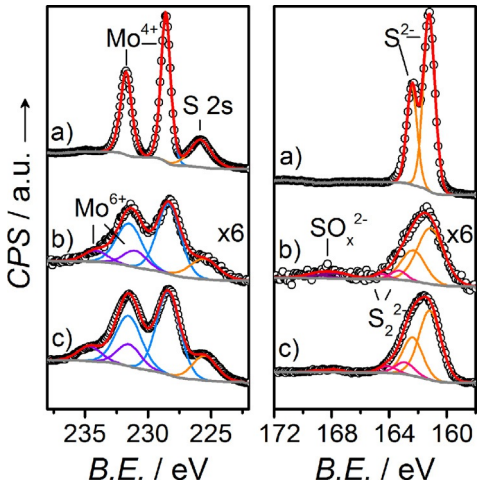

Figure 5. Fitted Mo 3d (left) and S 2p (right) XP spectra of a) bulk MoS_2 reference, b) MoS_2/TiO_2-RCP2-T, and c) MoS_2/TiO_2-RCP1. The data points are represented by open circles and the red lines represent the fits. The various contributions to the fit are labeled in the graphs. The spectra of MoS_2/TiO_2-RCP2 were magnified six times.

Table 2. Mo 3d XPS fit results.

Sample	Mo^{4+} BE [eV]	Mo^{6+} BE [eV]	Mo^{4+}[a] [%]	S/Mo[b]
MoS_2/TiO_2-RCP1	228.4	231.5	79	1.9
MoS_2/TiO_2-RCP2-T	228.4	231.2	81	2.1
MoS_2	228.9	–	100	2.1

[a] Calculated as $I_{Mo^{4+}}/(I_{Mo^{4+}} + I_{Mo^{6+}})$ where I is peak intensity. [b] Calculated as $I_{S_{red}}/I_{Mo^{4+}}$ where $I_{S_{red}}$ is the peak intensity of sulfur excluding sulfate.

action. The S 2p XP spectra are mainly composed of S^{2-} and S_2^{2-} species.[16] A small amount of oxidized S was also identified (SO_x^{2-}). This indicates that oxidized Mo and S species were likely formed by oxidation of MoS_2 during storage under ambient conditions. The sulfidation of Ti was not observed in the as synthesized samples. The stoichiometry of reduced sulfur to molybdenum for the samples prepared by RCP is comparable to that of bulk MoS_2 (Table 2), in line with the EDX results. A survey scan confirms that the as-synthesized catalysts are mainly composed of Mo, S, Ti, and O (Figure S3). Residual C and N species were also detected in the survey scan of the as-synthesized samples. In view of the low solubility of EDTA, we attribute this to the presence of EDTA in the as-synthesized materials. Nevertheless, EDTA thermally decomposes under the reaction conditions. Thus, we do not expect that it affected the catalytic properties of the materials.

Catalytic hydrodesulfurization properties

The catalytic activity and selectivity of samples prepared by RCP1 and RCP2 were evaluated in the liquid-phase HDS of dibenzothiophene (DBT) at 4.0 MPa and 245 °C. Desulfurization of DBT can proceed by two pathways as displayed in Scheme 1. Desulfurization of DBT by hydrogenolysis (DDS) yields biphenyl (BP) as the product, whereas hydrogenation of DBT followed by sulfur extraction (HYD) yields cyclohexylbenzene that can further be hydrogenated to bicyclohexane.

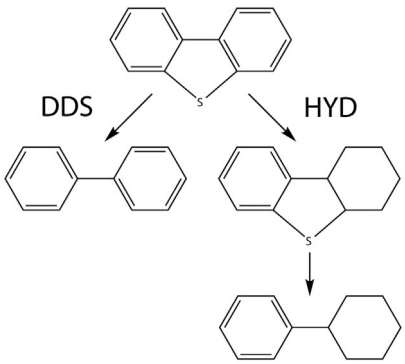

Scheme 1. Simplified mechanism of the desulfurization of DBT by direct desulfurization (DDS) or hydrogenation (HYD).

In Table 3, the results obtained from DBT activity tests of RCP and reference samples are reported. Additional selectivity (Figure S5) and Arrhenius plots (Figure S4) are provided in the Supporting Information. The reference samples were MoS_2 supported on P25 titania (65% anatase, 35% rutile) and a γ-Al_2O_3 supported commercial Co–Mo catalyst. Highest activities were obtained for unpromoted and Co-promoted MoS_2/TiO_2 prepared by RCP1, which exceeded the activity of the commercial reference with comparable metal loading. Catalysts prepared by RCP2 showed similar activity to the MoS_2/P25 reference, but were significantly less active than samples prepared by RCP1.

Table 3. Catalytic properties of the various samples in the liquid-phase HDS of DBT at 245 °C and 20 bar H_2.

Sample	k_{HDS} [a] [$g_{feed}\,g_{Mo}^{-1}\,h^{-1}$]	k_{BP} [b] $\times 10^4$ [$mol_{BP}\,mol_{Mo}^{-1}\,h^{-1}$]	HYD/DDS[c]	E_{Act} [d] [$kJ\,mol^{-1}$]
MoS_2/TiO_2-RCP1	9.1	0.85	27.9	170
Co-MoS_2/TiO_2-RCP1	12.1	6.1	4.4	128
MoS_2/TiO_2-RCP2-T	1.0	0.73	2.7	124
MoS_2/TiO_2-RCP2-H	n.m.	n.m.	n.m.	128
MoS_2/P25 impregnated[e]	1.3	0.55	5.4	115
commercial[f]	8.8	14.0	0.7	125

[a] Estimated error margin ±10%. [b] Rate constant for formation of biphenyl [c] Defined as ([Products]−[BP])/[BP]. [d] Arrhenius plots are presented in Figure S4. Estimated error margin ±10%. [e] Prepared by pore–volume impregnation, Mo loading 7.5 wt.% [f] Commercial Co–Mo/γ-Al_2O_3 catalyst containing ≈15 wt.% Mo.

The high activity of MoS_2/TiO_2-RCP1, as compared with that of the commercial catalyst, is remarkable since it does not contain a promoter. The sample was approximately eight times more active than MoS_2/TiO_2 prepared by impregnation or RCP2. However, the production rate constant of BP was similar for all unpromoted samples supported on TiO_2. The high activity obtained by the RCP1 method can thus be attributed to increased hydrogenation activity. The higher apparent activation energy of MoS_2/TiO_2-RCP1 points to a different formation mechanism of this sample compared to the others. If Co was present in the catalyst (Co–MoS_2/TiO_2-RCP1), the selectivity towards BP increased drastically whereas the overall rate only increased by 30%. The Mo loading remained constant, indicating that active HYD sites were replaced by DDS sites.

Several researchers have reported an increased hydrogenation activity of MoS_2 catalysts supported on TiO_2 versus those on other support materials.[11b,17] It has been proposed that Ti^{3+}, which may form under the reducing HDS conditions, could act as an electronic promoter in hydrogenation reactions over Ti–S–Mo sites.[17,18] Our results agree with this proposition, as addition of Co led to increased DDS activity at the expense of HYD activity. This suggests that Co resides at MoS_2 edge sites that would otherwise be promoted by Ti. Consequently, Co promotion in MoS_2/TiO_2 catalysts does not increase the overall HDS rate to the same extent as it does in γ-Al_2O_3-supported catalysts.[9c,17]

Despite the similar textural properties of catalysts prepared by RCP1 and RCP2, their morphologies as observed by TEM were obviously different. RCP2 and impregnated samples, which exhibited a relatively low hydrogenation activity, were prepared by depositing MoS_2 on a well-defined TiO_2 support. On the other hand, catalysts prepared by RCP1 were composed of coprecipitated MoS_2 and amorphous TiO_2. We anticipate that the RCP1 method yielded more Ti-promoted sites that are active in hydrogenation, which may explain the increased hydrogenation activity of these materials. Further studies in our laboratory aim to characterize the amorphous TiO_2 support and explore the unique activity of MoS_2/TiO_2-RCP catalysts in ultradeep HDS applications with real feed.

Conclusions

Unpromoted and cobalt-promoted molybdenum disulfide nanoparticles supported on titania were synthesized from aqueous solutions containing Ti and Mo precursor salts by an in situ redox reaction. The synthesis method, reductive coprecipitation (RCP), is simple and proceeds under mild conditions. Moreover, catalysts prepared by this way have higher Mo loading than those prepared by impregnation and their performance is comparable to that of commercial catalysts. Analysis by energy-dispersive X-ray spectroscopy indicated that the samples were composed of homogeneously dispersed MoS_2 nanoparticles on amorphous TiO_2. The morphology of TiO_2 could be controlled by synthesis of TiO_{2-x} prior to MoS_2 deposition, but this was at the expense of a lower Mo loading. Highest activities were obtained for the promoted RCP1 samples, which exceeded the performance of a commercial reference in hydrodesulfurization of dibenzothiophene. The addition of Co as a promoter did not enhance the catalytic activity of MoS_2/TiO_2 to the same extend (+30%) as for Al_2O_3-supported Co–Mo catalysts. However, the promoter changed the selectivity towards hydrogenolysis products at the expense of hydrogenation products. These results point to the substitution of Ti-promoted sites by Co-promoted sites upon addition of Co.

Experimental Section

Materials preparation

A detailed description of the materials synthesis is provided in the Supporting Information. Key aspects of the synthesis are given below. The RCP synthesis procedure was modified from Xie et al.[5a] MoS_2/TiO_2-RCP1 was synthesized from aqueous solutions of $TiCl_3$ and $(NH_4)_2MoS_4$ at 100 °C. The promoted material, Co–MoS_2/TiO_2-RCP1, was synthesized by the same procedure with $Co(NO_3)_2{\cdot}6H_2O$ added to the $TiCl_3$ solution. For the preparation of RCP2 materials, TiO_{2-x} was synthesized first by thermolysis (T) or hydrolysis (H). In thermolysis, TiO_{2-x} was formed overnight at 60 °C from an aqueous solution of $TiCl_3$ in HCl, stabilized by NaCl. In hydrolysis, TiO_{2-x} was formed overnight at 60 °C by basification of acidic $TiCl_3$ solution with NaOH (1 M). TiO_{2-x} was filtered and washed and redispersed in water. MoS_2/TiO_2-RCP2 materials were then synthesized by addition of an aqueous $(NH_4)_2MoS_4$ solution to the suspension of TiO_{2-x} under inert conditions.

Characterization

N_2 adsorption isotherms were measured at −196 °C on a Micromeretics Tristar II. Prior to analysis, samples were heated at 160 °C for

4 h under flowing N_2. Specific surface areas were determined by the BET method. TEM measurements were made with a Tecnai-20F microscope operated at 200 kV and equipped with a field-emission gun. EDX spectroscopy was performed on the same microscope, utilizing an EDAX analyzer with TIA software. XRD patterns were recorded with a PANalytical X'pert PRO powder diffractometer equipped with a sealed Cu anode tube, operated at 45 kV and 40 mA. Samples were ground with a mortar and pestle prior to analysis. XPS was performed with a Kratos AXIS Ultra spectrometer, equipped with a monochromatic X-ray source and a delay-line detector. Spectra were obtained by using the aluminium anode ($Al_{K\alpha}$ = 1486.6 eV). Survey scans were measured at a constant pass energy of 160 eV and region scans at 40 eV. The background pressure was 2×10^{-9} mbar. Energy correction was performed by using the C 1s peak at 284.6 eV as a reference. X-ray fluorescence (XRF) was recorded with a PANalytical spectrometer equipped with a MagiX Pro (PW2440). Samples were mixed with Al_2O_3 and a glass bead was sintered for analysis.

Catalytic hydrodesulfurization activity

The catalytic activity was determined by means of DBT HDS in a fixed-bed high-pressure tubular reactor with a down-flow (trickle flow) of gas and liquid feed (40 bar, H_2 flow of 2.25 mL min^{-1}, weight hourly space velocity of 1.4 h^{-1}). The reactor, 240 mm in length and 4 mm in diameter (ID), was packed with 30–80 mesh catalyst particles (400 mg) sandwiched between two ZrO_2 layers. The catalysts were pretreated with *n*-hexadecane (Sigma–Aldrich) spiked with 5.2% tetranonyl pentasulfide (Sigma–Aldrich) at 280 °C for 5 h and subsequently at 340 °C for 24 h. Afterwards, the temperature was lowered to 200 °C for 8 h. Then, the feed was switched to the reaction feed (5 wt.% DBT, 2 wt.% adamantane in *n*-hexadecane). After equilibration for 2 h, the temperature was increased to the desired reaction temperature (245 °C). Steady-state activity was measured after 24 h of reaction by offline GC-FID.

Acknowledgements

We thank A. Soula for the DBT activity tests and we thank A. J. F. van Hoof and W. L. Vrijburg for fruitful discussions.

Keywords: desulfurization · molybdenum · nanoparticles · redox chemistry · supported catalysts

[1] *Preparation of solid catalysts* (Eds.: G. Ertl, H. Knözinger, J. Weitkamp), Wiley-VCH, Weinheim, Germany, **1999**.
[2] *Synthesis of solid catalysts* (Ed.: K. P. de Jong), Wiley-VCH, Weinheim, **2009**.
[3] a) N. Zheng, G. D. Stucky, *J. Am. Chem. Soc.* **2006**, *128*, 14278–14280; b) J. Blanco, A. L. Petre, M. Yates, M. P. Martin, S. Suarez, J. A. Martin, *Adv. Mater.* **2006**, *18*, 1162–1165; c) R. J. White, R. Luque, V. L. Budarin, J. H. Clark, D. J. Macquarrie, *Chem. Soc. Rev.* **2009**, *38*, 481–494.
[4] a) Z. C. Wang, Y. J. Jiang, R. Rachwalik, Z. W. Liu, J. Shi, M. Hunger, J. Huang, *ChemCatChem* **2013**, *5*, 3889–3896; b) C. Sprung, B. Arnstad, U. Olsbye, *ChemCatChem* **2014**, *6*, 1969–1982; c) J. M. Campelo, D. Luna, R. Luque, J. M. Marinas, A. A. Romero, *ChemSusChem* **2009**, *2*, 18–45.
[5] a) Y. Xie, K. Ding, Z. Liu, R. Tao, Z. Sun, H. Zhang, G. An, *J. Am. Chem. Soc.* **2009**, *131*, 6648–6649; b) S. Golunski, R. Rajaram, N. Hodge, G. J. Hutchings, C. J. Kiely, *Catal. Today* **2002**, *72*, 107–113.
[6] W. Ho, J. C. Yu, J. Lin, J. Yu, P. Li, *Langmuir* **2004**, *20*, 5865–5869.
[7] M. Chhowalla, H. S. Shin, G. Eda, L. J. Li, K. P. Loh, H. Zhang, *Nat. Chem.* **2013**, *5*, 263–275.
[8] R. Prins in *Handbook of Heterogeneous Catalysis, Vol. 6* (Eds.: G. Ertl, H. Knozinger, F. Schuth, J. Weitkamp), Wiley-VCH, Weinheim, **2008**, pp. 2696–2718.
[9] a) M. Breysse, C. Geantet, P. Afanasiev, J. Blanchard, M. Vrinat, *Catal. Today* **2008**, *130*, 3–13; b) K. Y. S. Ng, E. Gulari, *J. Catal.* **1985**, *92*, 340–354; c) J. Ramirez, S. Fuentes, G. Diaz, M. Vrinat, M. Breysse, M. Lacroix, *Appl. Catal.* **1989**, *52*, 211–224.
[10] a) S. Dzwigaj, C. Louis, A. Breysse, M. Cattenot, V. Belliere, C. Geantet, M. Vrinat, P. Blanchard, E. Payen, S. Inoue, H. Kudo, Y. Yoshimura, *Appl. Catal. B* **2003**, *41*, 181–191; b) J. A. Toledo-Antonio, M. A. Cortes-Jacome, C. Angeles-Chavez, J. Escobar, *Appl. Catal. B* **2009**, *90*, 213–223.
[11] a) A. Guevara, A. Alvarez, M. Vrinat, *Catal. Lett.* **2008**, *126*, 268–274; b) M. C. Barrera, J. Escobar, C. Marin, M. Viniegra, J. A. D. L. Reyes, J. G. Pacheco, F. Murrieta, *Pet. Sci. Technol.* **2004**, *22*, 87–101; c) Z. L. Zhang, Y. S. Zhou, S. J. Zhang, C. M. Xu, *Energy Fuels* **2006**, *20*, 2293–2298; d) W. Q. Huang, A. J. Duan, Z. Zhao, G. F. Wan, G. Y. Jiang, T. Dou, K. H. Chung, J. Liu, *Catal. Today* **2008**, *131*, 314–321.
[12] Z. B. Wei, W. H. Yan, H. Zhang, T. L. Ren, Q. Xin, Z. C. Li, *Appl Catal a-Gen* **1998**, *167*, 39–48.
[13] D. L. Nguyen, S. Gillot, D. O. Souza, P. Blanchard, L. Chamonier, E. Berrier, T. V. Kotbagi, M. K. Dongare, S. M. Umbarkar, S. Cristol, E. Payen, C. Lancelot, *ChemCatChem* **2012**, *4*, 2112–2120.
[14] a) A. Di Paola, G. Cufalo, M. Addamo, M. Bellardita, R. Campostrini, M. Ischia, R. Ceccato, L. Palmisano, *Colloids Surf. A* **2008**, *317*, 366–376; b) S. Cassaignon, M. Koelsch, J.-P. Jolivet, *J. Phys. Chem. Solids* **2007**, *68*, 695–700; c) T. H. Wang, A. M. Navarrete-Lopez, S. G. Li, D. A. Dixon, J. L. Gole, *J. Phys. Chem. A* **2010**, *114*, 7561–7570.
[15] a) Th. Weber, J. C. Muijsers, J. W. Niemantsverdriet, *J. Phys. Chem.* **1995**, *99*, 9194–9200; b) P. Afanasiev, G. F. Xia, G. Berhault, B. Jouguet, M. Lacroix, *Chem. Mater.* **1999**, *11*, 3216–3219.
[16] J. C. Muijsers, Th. Weber, R. M. v. Hardeveld, H. W. Zandbergen, J. W. Niemantsverdriet, *J. Catal.* **1995**, *157*, 698–705.
[17] L. Coulier, J. A. R. v. Veen, J. W. Niemantsverdriet, *Catal. Lett.* **2002**, *79*, 149–155.
[18] J. Ramírez, G. Macías, L. Cedeno, A. Gutiérrez-Alejandre, R. Cuevas, P. Castillo, *Catal. Today* **2004**, *98*, 19–30.

Received: December 9, 2015
Published online on February 23, 2016